J. Fluid Mech. (2003), *vol.* 482, *pp.* 235–255.
DOI: 10.1017/S0022112003004026 Printed in the United Kingdom

Trapped vortices and a favourable pressure gradient

By S. I. CHERNYSHENKO[1], B. GALLETTI[2], A. IOLLO[2] AND LUCA ZANNETTI[2]

[1]School of Engineering Sciences, University of Southampton, Southampton, SO17 1BJ, UK

[2]Dipartimento di Ingegneria Aeronautica e Spaziale, Politecnico di Torino, Torino, Italy

(Received 17 June 2002 and in revised form 1 December 2002)

It is shown that there exist bodies such that in two-dimensional steady inviscid incompressible flow the pressure gradient is favourable over the entire surface of the body, and the lift is non-zero, if the body is immersed in a uniform stream and there are also two trapped point vortices.

1. Introduction

In flows of practical importance, the Reynolds number is often fairly large. With Reynolds number being the ratio of inertial and viscous forces, this means that viscosity effects can sometimes be neglected. The theory of inviscid flows is substantially simpler than the theory of viscous flows. Many useful results have been obtained within the inviscid flow theory, the most noteworthy of which is probably the theory of lift.

A major limitation on the use of inviscid flow theory is imposed by separation. Separation is a predominantly viscous phenomenon. In non-separated flows, viscosity effects are confined to thin boundary layers adjacent to the walls. In separated flows these thin layers protrude into the flow. Even in this case they can be modelled as vortex sheets within the inviscid flow theory. However, inviscid models of separated flow possess an intrinsic non-uniqueness when separation occurs from a smooth wall. In an ideal fluid flow, the position of the separation point can be prescribed arbitrarily within certain limits, while in a real flow it is determined by viscous effects. If the flow is assumed to be two-dimensional and steady then there is an additional source of non-uniqueness of the inviscid separated flow models. In a non-separated steady flow, all the streamlines come from infinity. The vorticity is constant along the streamlines and its distribution across the streamlines can be determined from the boundary conditions at infinity. In steady separated flows, streamlines form closed contours in the eddy. Therefore, the vorticity on closed streamlines cannot be determined from the boundary conditions. Instead, the distribution of vorticity is governed by viscous effects, however small they are, as demonstrated by the Prandtl–Batchelor theorem, see Batchelor (1956). In addition to the difficulties of the theoretical description of separated flows, separation of the flow past a wing leads to an increase in drag and often to a decrease in lift. For these reasons, separation is avoided in airfoil shape design.

Exact criteria of separation are difficult to obtain. In the case of a laminar flow, it is possible to calculate a boundary layer and thus at least check whether separation occurs for a given inviscid velocity distribution along the body surface. In the more

practically important case of a turbulent boundary layer, such calculations can only be approximate. On the other hand, both the boundary layer theory and practical observations show that a boundary layer never separates when the pressure does not increase in the direction of the flow. For this reason a negative pressure gradient is called favourable. Therefore, in order to avoid separation, it is sufficient to ensure that the pressure gradient is favourable or zero over the entire body surface. A flat plate aligned with the flow direction is an example of such a body. However, it does not create lift and it has zero volume.

Designing a body shape with a favourable pressure gradient over the entire surface is of substantial practical and theoretical interest. At a first glance, the airfoil theory inverse problem methods (Lighthill 1945; Elizarov, Il'inskiy & Potashev 1997) would seem to be suitable to achieve this goal. The inverse problem is that of determining the airfoil shape for a given velocity distribution on its surface. The major feature of the inverse problem is that, if the velocity distribution is prescribed arbitrarily, the resulting airfoil contour is not closed, and the corresponding potential flow occurs on a multivalent Riemann surface. The additional constraint of the airfoil contour being closed can be satisfied if a three-parameter family of velocity distributions is given so that the solution to the inverse problem determines both the airfoil shape and the values of the parameters that correspond to that shape. It is possible to prescribe a family that only consists of velocity distributions with favourable pressure gradients, and the corresponding closed airfoil contour can be obtained. However, in all attempts the resulting airfoil contours are self-intersecting, even though the overlap of the upper and lower surfaces of the airfoil can be small. This is a general result: according to the Stepanov theorem, see Avhadief & Maklakov (1995), a potential flow past a body necessarily creates an unfavourable pressure gradient on at least one portion of the body surface.

Under certain circumstances, separation can be acceptable and even useful. An example of this is airfoils with trapped vortices. The idea of such an airfoil is to ensure, in some way, that the separated vortex remains permanently in the vicinity of the airfoil and is not shed downstream and replaced periodically (or chaotically) with a new vortex. High drag and low lift, usually observed at a high angle of attack, are in fact due to this periodic or chaotic vortex shedding but not to the separation itself. Vortex-trapping airfoils have been studied both theoretically and in experiments for a long time, mainly as a means of enhancing lift and preventing or controlling separation (see Saffman & Sheffield 1977; Rossow 1978; Huang & Chow 1982; Wu & Wu 1992; Bunyakin, Chernyshenko & Stepanov 1998 where further references can be found; Baranov *et al.* 2000). Vortex control is dealt with in Chernyshenko (1995), Wu *et al.* (1998) and Iollo & Zannetti (2000). It is important to note that a favourable pressure gradient at rigid boundaries is also desirable for flows with trapped vortices. In this case an adverse pressure gradient can lead to secondary separation, resulting in an increased number of eddies, and flows with multiple eddies are more difficult to calculate and more likely to be unstable. It was shown in Bunyakin *et al.* (1998) however that, for a wide class of eddy shapes, the pressure distribution has at least two maxima and two minima on the eddy boundary, thus making it unlikely that airfoils with one trapped vortex can have a favourable pressure gradient over the entire rigid surface.

More details will be given on this at the end of the paper. In § 2 we extend the Stepanov theorem to airfoils with unbounded curvature and formulate certain specific results concerning the behaviour of the solutions near the trailing edge at which the velocity maximum is attained. Section 3, which is very short, is devoted to airfoils

with a single trapped vortex. Section 4 contains the main result of the present paper: an example of a lifting body with two trapped point vortices and with a favourable pressure gradient over the entire rigid surface. The concluding discussion section gives a concise formulation of the newly obtained results and highlights the yet unsolved problems which could be of interest in view of these results. The flow is considered to be ideal two-dimensional, steady, and incompressible throughout the paper, with real flow effects only mentioned in the introduction and discussion sections.

2. Stepanov theorem

2.1. *Airfoils with unbounded curvature*

The incompressible potential flow past a single airfoil in complex z-plane, $z = x + \mathrm{i}y$, is considered. The Stepanov theorem (Elizarov *et al.* 1997) states that a favourable pressure distribution over the entire airfoil surface is impossible. This theorem has been proved (Avhadief & Maklakov 1995) for smooth airfoils of finite curvature. We will extend the proof to the case when the curvature tends to infinity near the trailing edge. The incentive for doing this is that when the velocity distribution over the airfoil surface is prescribed and the airfoil shape is being sought as the solution to the inverse boundary-value problem, the resulting shape often has infinite curvature near the cusp. (An airfoil with a favourable pressure gradient near the trailing edge must have a cusped trailing edge to avoid stagnation.) Let us consider, for example, a symmetric airfoil at zero incidence and assume that the velocity on the airfoil surface is constant in the vicinity of the cusp. Therefore, the angle between the airfoil surface and the trailing streamline at the trailing edge in the hodograph plane is 90° while it is 180° in the physical space. This immediately leads to infinite curvature.

The Stepanov theorem can be proved by *reductio ad absurdum*. We assume that the pressure gradient is favourable everywhere on the airfoil surface and prove that, in this case, the airfoil contour has self-intersections.

Let $w(z)$ be the complex potential of the flow. The complex velocity $\mathrm{d}w/\mathrm{d}z = V_p(z)$ is analytic in the region exterior to the airfoil. The Riemann mapping theorem guarantees that such a domain can be thought of as the region exterior to the unit circle in a complex μ-plane, $\mu = \rho\exp(\mathrm{i}\varphi)$, mapped to the z-plane by an analytic function $z = z(\mu)$ so that $\lim_{\mu\to\infty} z = \infty$. It follows that the complex velocity V_p is an analytic function of μ as well, i.e. $V_p = V_p(\mu)$. Without loss of generality, we may assume that the trailing edge is at $z = 0$, and that it corresponds to $\mu = 1$ in the μ-plane, with the velocity at the trailing edge directed along the x-axis.

Let $V_p = |V_p|\exp(-\mathrm{i}\omega)$, with ω denoting the flow velocity angle on the physical z-plane. A favourable pressure gradient everywhere on the surface, from the forward stagnation point to the trailing edge, implies that the flow velocity reaches its maximum value at the trailing edge. Since, according to the maximum modulus principle, $|V_p|$ attains its maximum over the entire flow domain at a point of the unit circle, this point is at the trailing edge $\mu = 1$.

Therefore, at this point, according to the Hopf boundary-point lemma, see Courant (1962),

$$\frac{\partial|V_p|}{\partial\rho} < 0. \tag{2.1}$$

Here, the derivative at $\mu = 1$ can be understood as the upper bound of $\partial|V_p|/\partial\rho$ as $\mu \to 1$. From the Cauchy–Riemann conditions applied to $\log V_p(\mu)$ as a function

FIGURE 1. Airfoil with a favourable pressure gradient on the entire surface.

of $\log\mu$

$$\frac{\partial\omega}{\partial\varphi} = -\rho\frac{\partial\log|V_p|}{\partial\rho}. \tag{2.2}$$

From this and (2.1) it follows that as $\mu \to 1$, the lower bound of $\partial\omega/\partial\varphi$ is strictly positive. Therefore, there exists a constant $C > 0$ such that on the unit circle ($\rho = 1$)

$$\omega(\varphi) > C\varphi, \quad \varphi > 0; \qquad \omega(\varphi) < C\varphi, \quad \varphi < 0 \tag{2.3}$$

in a certain vicinity of the point $\mu = 1$.

Near the cusp $z = A(\mu-1)^2 + \cdots$ with the real constant $A > 0$, so that on the airfoil surface $x = -A\varphi^2 + \cdots$. When a point in the μ-plane moves anticlockwise around the unit circle the corresponding point in the physical plane moves anticlockwise around the airfoil, with the airfoil being to the left of the direction of the point motion. We will refer to points with $\varphi < 0$ (>0) in the vicinity of the trailing edge as the lower (upper) airfoil surface. This convention corresponds to an approximately horizontal airfoil with the trailing edge at the right-hand end of it. Then $\varphi = \pm\sqrt{-x/A} + \cdots$ at the lower ($-$) and upper ($+$) surfaces. Let the lower (upper) surface be $y = Y_-(x)$ ($y = Y_+(x)$) near the trailing edge. At the airfoil surface $\mathrm{d}y/\mathrm{d}x = \tan\omega$. Therefore

$$Y_\pm(x) = \int_0^x \tan\omega(\varphi)\,\mathrm{d}x = \int_0^x \tan\omega(\pm\sqrt{-x/A} + \cdots)\,\mathrm{d}x.$$

Hence

$$Y_+(x) - Y_-(x) = \int_0^x \left[\tan\omega(\sqrt{-x/A} + \cdots) - \tan\omega(-\sqrt{-x/A} + \cdots)\right]\,\mathrm{d}x$$

and, using (2.3) and recalling that $x < 0$,

$$Y_+(x) - Y_-(x) < 2\int_0^x \tan C\sqrt{-x/A}\,\mathrm{d}x < 0.$$

That is, we have showed that if the maximum velocity is attained at the trailing edge, the upper airfoil surface is below the lower airfoil surface, see figure 1. This proves the Stepanov theorem.

It should be noted that this proof has to be modified if the maximum is attained at more than one point, as is the case if, when solving the inverse boundary-value problem, constant $|V_p|$ is prescribed on a finite section of the airfoil in the vicinity of the trailing edge. This special case can be treated by using the hodograph plane to obtain and analyse a local solution near the trailing edge.

Let us now consider how the Stepanov theorem was proved in Avhadiev & Maklakov (1995). Denoting the profile arclength s and assuming the airfoil curvature radius $R \neq 0$, one obtains

$$\left(\frac{\partial\omega}{\partial\varphi}\right)_{\varphi=0} = \frac{\partial\omega}{\partial s}\frac{\mathrm{d}s}{\mathrm{d}\varphi} = \frac{1}{R}\left|\frac{\mathrm{d}z}{\mathrm{d}\mu}\right| = 0 \tag{2.4}$$

at the trailing edge. It therefore follows from (2.2) that $\partial|V_p|/\partial\rho$ exists and is equal to zero at $\mu = 1$ thus violating the Hopf boundary-point lemma. The proof given in the present paper is, therefore, just a simple enhancement obtained using the stronger formulation of the Hopf lemma which is applicable even when $\partial|V_p|/\partial\rho$ does not exist at $\mu = 1$ in the ordinary sense.

2.2. *Necessary condition for a favourable pressure gradient*

As the proof given in the preceding section indicates, allowing the airfoil or the flow in question to exhibit irregularity at the trailing edge does not ensure any advantages with respect to the pressure gradient being favourable. For this reason, and also since this assumption is sufficient for our further considerations, we assume now that $|V_p|$ is a smooth function of φ with at least two derivatives on the unit circle in the μ-plane. The Stepanov theorem can then be reformulated briefly by stating that, according to the Hopf lemma, the critical points pertinent to modular surfaces of analytic functions cannot be elliptic, while, *absurde*, it would be the case if $\max|V_p|$ were attained at the trailing edge $\mu = 1$. Nevertheless, a hyperbolic critical point is not forbidden at $\mu = 1$. In this case, the modular surface $|V_p|$ has a saddle at $\mu = 1$, with a local maximum with respect to the profile points ($\partial|V_p|/\partial\varphi = 0$) and a local minimum with respect to the exterior points ($\partial|V_p|/\partial\rho = 0$). Under the Stepanov theorem assumption that the flow is potential exterior to the airfoil, such an occurrence is of little help in gaining a favourable pressure gradient everywhere since, according to the maximum modulus principle, the absolute maximum should be reached at another point on the profile contour. However, in principle and *de facto*, as will be shown in what follows, a trailing-edge hyperbolic critical point can ensure a favourable pressure gradient everywhere on an airfoil if there is some vorticity inside the flow field, for instance in the form of a point vortex. In this case, the maximum modulus principle does not apply and the velocity can increase monotonically from the stagnation point to a cusped trailing edge where it reaches the maximum value along the boundary values without violating the Stepanov theorem.

In this case

$$\left(\frac{\partial|V_p|}{\partial\varphi}\right)_{\text{trailing edge}} = 0, \tag{2.5}$$

at the trailing edge, providing the *necessary condition for the pressure gradient to be favourable everywhere on the profile contour* and without any inconsistency with (2.4).

The parametric representation $|V_p| = |V_p|(\varphi)$ of the flow velocity on the profile, as a function of the transformed unit circle angle, provides a simple tool to reveal the flow behaviour in the vicinity of a cusped trailing edge. The derivative of the flow velocity, with respect to the profile arclength s, is given by

$$\frac{\mathrm{d}|V_p|}{\mathrm{d}s} = \frac{\partial|V_p|/\partial\varphi}{|\mathrm{d}z/\mathrm{d}\mu|}. \tag{2.6}$$

At a cusped trailing edge, $\mathrm{d}z/\mathrm{d}\mu = 0$ and $V_p \neq 0$. If a local maximum is reached, (2.6) is indeterminate, and its limiting value is

$$\frac{\mathrm{d}|V_p|}{\mathrm{d}s} = \lim_{\varphi\to 0}\frac{\partial|V_p|/\partial\varphi}{|\mathrm{d}z/\mathrm{d}\mu|} = \left(\frac{\partial^2|V_p|/\partial\varphi^2}{(\partial/\partial\varphi)\,|\mathrm{d}z/\mathrm{d}\mu|}\right)_{\varphi=0}.$$

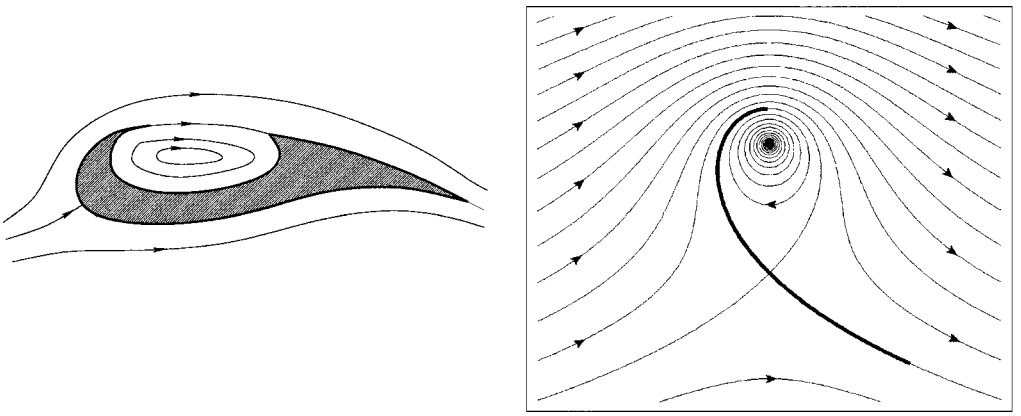

FIGURE 2. Vortex-trapping airfoil and its idealized model.

The denominator of this limit value can be different from zero. Assuming that the mapping $z(\mu)$ can be expanded about the trailing edge as

$$z = \left(1 - \frac{1}{\mu}\right)^2 \sum_{n=0}^{\infty} c_n(\mu - 1)^n \qquad (c_0 \neq 0),$$

the limit of $\partial|\mathrm{d}z/\mathrm{d}\mu|/\partial\varphi$ is

$$\lim_{\varphi \to 0^{\pm}} \frac{\partial}{\partial \varphi} \left|\frac{\mathrm{d}z}{\mathrm{d}\mu}\right| = \pm 2|c_0|.$$

Thus, the flow has opposite finite gradients on both sides if $\partial^2|V_p|/\partial\varphi^2 \neq 0$ or zero gradient if $\partial^2|V_p|/\partial\varphi^2 = 0$.

If a local velocity maximum is not reached, $\partial|V_p|/\partial\varphi$ has the same sign on the two cusp sides. It follows that the pressure gradient is favourable on one side and unfavourable on the other side, and it tends to infinity as the cusp is approached.

This has certain implications for airfoil design methods. One could start with a certain airfoil and vary its shape in some kind of optimization procedure, with the maximum value of the adverse pressure gradient as the functional which is to be minimized. However, such an approach is not feasible since this functional is indefinite.

3. Vortex-trapping airfoils

The idea that the presence of a vortex region near an airfoil can improve the airfoil performance is quite old. The so-called vortex-trapping airfoil is illustrated in figure 2 together with its highly idealized point-vortex model. Ideally, the pressure should decrease along the entire lower surface, and it also should decrease from the stagnation point to the cusp at the start of the cavity; then it may increase along the separating streamline, and, after reattachment, only decrease along the wall toward the trailing edge and back along the cavity wall toward the separation point.

The idealized model streamline pattern shown in figure 2 is due to a vortex with clockwise circulation and a free stream in the direction of the positive real axis. The marked bold streamline arc behaves as a zero thickness airfoil with two cusps at its ends when considered as solid. The flow accelerates monotonically from the stagnation points to the cusps on both sides.

However, the vortex in figure 2 is not in equilibrium, therefore such a flow is not a valid example of a physically possible steady flow with a favourable pressure gradient, even from a very ideal point of view. The example is nevertheless useful since it shows that an airfoil that is capable of trapping a standing vortex could have a favourable pressure gradient without having self-intersections.

Since the vortex is not in equilibrium it exerts a force on the fluid. This is a substantial point since, as a consequence of the theorem proved in Bunyakin *et al.* (1998), if the vortex is in equilibrium then either there are more than one pressure maximum and one pressure minimum on the streamline encircling the vortex, or the vortical region has a very complex shape. It was shown in Bunyakin *et al.* (1998) that if the pressure on the boundary of the closed streamline region has only one minimum and one maximum, as implied by our idealized picture, then the total pressure force exerted at this boundary is non-zero. (The force exerted by the vortex on the fluid in figure 2 is of course exactly equal to the pressure force exerted on the eddy boundary, so that the centre of mass of fluid in the eddy remains at rest.) This theorem is proved for quite a wide class of eddy shapes: this class consists of all those shapes where a circle can be drawn through any two points on its boundary without other intersections with this boundary. This, naturally, includes any convex shape.

Note now that the proof in Bunyakin *et al.* (1998) cannot be extended to arbitrary shapes. It is in fact possible to construct an example of an S-shaped region and a pressure distribution with only one minimum and one maximum on it so that both the total pressure force and the total moment of the pressure force are zero. It is of course quite probable that such a pressure distribution could never occur in a fluid flow. It might also be possible to have an eddy of a simple shape but such that these inevitable additional pressure minimum and maximum are located on the separating streamline, so that the pressure gradient at the rigid walls is favourable everywhere. However, no examples of such a flow are as yet known.

Although, in real flows with closed streamlines, the vorticity is distributed inside the eddy, a potential flow with a point vortex obviously captures both difficulties associated to the Stepanov theorem and the theorem in Bunyakin *et al.* (1998) and is much easier to calculate. For this reason, point-vortex models are in principle suitable for studying the feasibility of various approaches to the design of airfoils with a favourable pressure gradient. Due to the strong limitations imposed by these theorems, it is clear that the trial-and-error approach is not very likely to succeed. This is why an attempt was made to solve the inverse boundary-value problem for vortex-trapping airfoils by Galletti, Iollo & Zannetti (2002), who gave an analytical method to design vortex-trapping airfoils. Their method is inspired by the Elizarov *et al.* (1997) method to solve inverse problems for simple airfoils. It makes it possible to find the shape that a vortex-trapping airfoil should have to obtain a velocity distribution which is as close, in a certain sense, as possible to the distribution prescribed along its contour.

A solution to the problem of finding an airfoil with a favourable pressure gradient could be attempted with Galletti *et al.*'s (2002) method by prescribing an appropriate velocity distribution and then solving the pertinent inverse problem. The main difficulty is that airfoil inverse problems are usually ill-posed and solvability condition have to be enforced (Lighthill 1945; Elizarov *et al.* 1997). Galletti *et al.* (2002) have shown that the inverse vortex-trapping airfoil problem is well-posed when the design velocity satisfies five integral constraints, of which three are equivalent to the three (Lighthill 1945) constraints for consistency with velocity at infinity and airfoil closure,

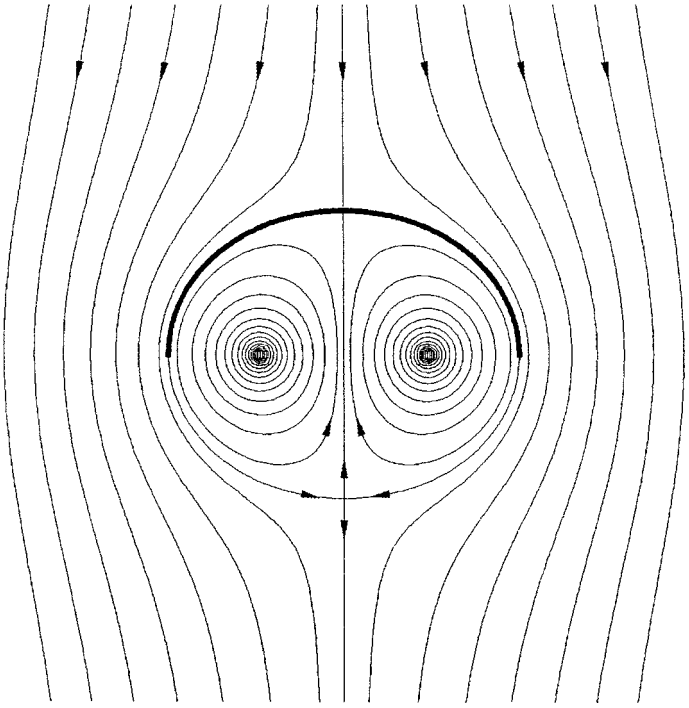

FIGURE 3. The streamline pattern for a vortex pair superimposed on a uniform flow.

while another two constraints are needed to guarantee vortex equilibrium. As in Elizarov *et al.* (1997), once an arbitrary design velocity distribution is chosen, the problem is solved for a modified distribution which, according to a variational criterion, is the closest one that satisfies the constraints. Our attempts to solve the problem of a favourable-pressure-gradient airfoil by these means failed. The main reason for this failure, besides the difficulty of avoiding airfoil self-intersection, appeared to be that the necessary condition (2.5) has to be exactly satisfied; the variational closest concept is of little help for this purpose. Because of the severe limitation on the eddy shape, as imposed by the theorem proved in Bunyakin *et al.* (1998), a favourable-pressure-gradient airfoil with a single trapped vortex could be impossible.

4. Lifting body with two trapped vortices

4.1. *Vortex pair*

A consistent example of a favourable-pressure-gradient body is given by the vortex-pair flow. The streamline pattern for a vortex pair superimposed on an uniform flow, directed in the sense of the negative imaginary axes, is shown in figure 3. It is characterized by a closed streamline that separates the fluid entrained by the vortices from the rest of the fluid. A properly selected segment of this separatrix, as shown in bold in figure 3, can act as a doubly cusped zero-thickness profile that traps a vortex pair and has a favourable pressure gradient everywhere on the profile. The resulting trailing-edge velocity gradients can be finite or zero, depending on the choice of segment extrema, in agreement with the analysis in § 2.2. Notice that, in this case, the vortices are in equilibrium.

This example proves the existence of a steady flow past a body with a favourable pressure gradient everywhere on the body surface, but it is of limited interest since such a body has no thickness and does not produce lift. The question now is: does a thick lifting body with a pressure gradient favourable everywhere on its surface exist? We answer the question positively by providing an example of a body with such properties.

The process we follow is based on conformal mapping. In brief, a thick profile is generated by modifying an arc of the vortex pair separatrix. The profile is then mapped from the physical z-plane onto the unit circle in the μ-plane, where the complex potential is determined. Free flow parameters exist that are adjusted by means of a conjugate gradient descent method in order to satisfy the necessary conditions for flows with a favourable pressure gradient. The fulfilment of the goal of an everywhere-favourable pressure gradient is verified *a posteriori*.

4.2. *Profile generation and mapping*

The complex potential pertinent to the vortex-pair flow of figure 3 is:

$$w_v = \mathrm{i}z + \frac{\kappa}{2\pi\mathrm{i}} \log\left(\frac{z - x_0}{z + x_0}\right), \tag{4.1}$$

where, at infinity, the flow has unit velocity and is in the same direction as the negative imaginary axis. The two opposite vortices, whose circulations are κ and $-\kappa$, are located on the real axis at $x = x_0$ and $x = -x_0$. The vortices do not move when $\kappa = -4\pi x_0$. The separatrix equation is

$$S(x, y) = \mathrm{Im}(w_v) = 0. \tag{4.2}$$

Let x_L denote the intersection of the separatrix and the real axis. The ratio $\eta = x_L/x_0$ is therefore the solution of equation

$$\eta + 2\log\left(\frac{\eta - 1}{\eta + 1}\right) = 0,$$

that is, $\eta = 2.08725$. We assumed $x_L = 1$, obtaining $x_0 = 1/\eta$, $\kappa = -4\pi/\eta$.

To generate the profile, a separatrix arc $z_s = x_s + \mathrm{i}y_s$ is first selected by choosing its extrema z_{T_1}, z_{T_2}. The arc is then computed as a set of points that are determined by solving the polar representation of equation (4.2) using a trial-and-error process. An example is shown in figure 4 for the choice of $\arg(z_{T_1}) = 5°$, $\arg(z_{T_2}) = 180° - 5°$.

The inner side $z_v = x_v + \mathrm{i}y_v$ of the profile is obtained by deforming this separatrix arc without altering its extrema z_{T_1}, z_{T_2}. The deformation is carried out according to the equations

$$x_v = x_s, \quad y_v = y_s + \sigma \sin\left(2\pi \frac{x_s - x_{T_2}}{x_{T_1} - x_{T_2}}\right),$$

where σ is the deformation maximum amplitude. The altered arc corresponding to $\sigma = 0.06$ is superimposed onto the original arc in figure 4.

The outer profile contour $z_d = x_d + \mathrm{i}y_d$ is obtained by adding a thickness distribution to the inner contour according to the law

$$x_d = x_v, \quad y_d = y_v + \epsilon \exp\left(\frac{\chi}{x_v - x_{T_1}} - \frac{1 - \chi}{x_v - x_{T_2}}\right), \tag{4.3}$$

where $\epsilon > 0$ and $0 < \chi < 1$. The thickness distribution (4.3) is such that the profile

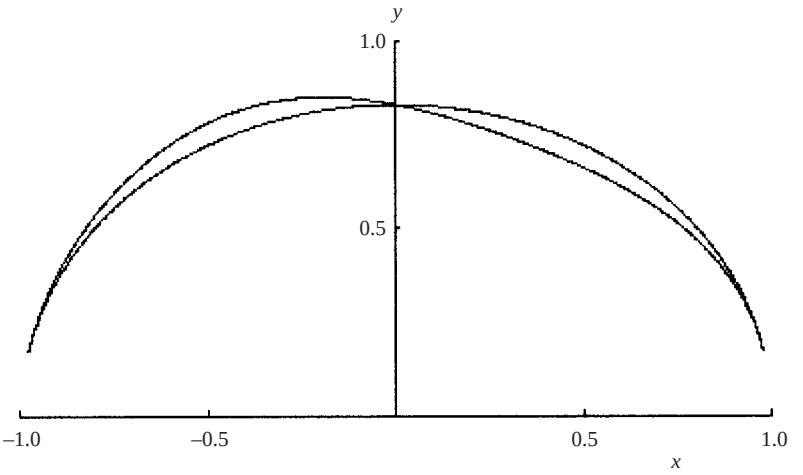

FIGURE 4. Separatrix arc ($\arg(z_{T_1}) = 5°$, $\arg(z_{T_2}) = 180° - 5°$) and modified arc ($\sigma = 0.06$).

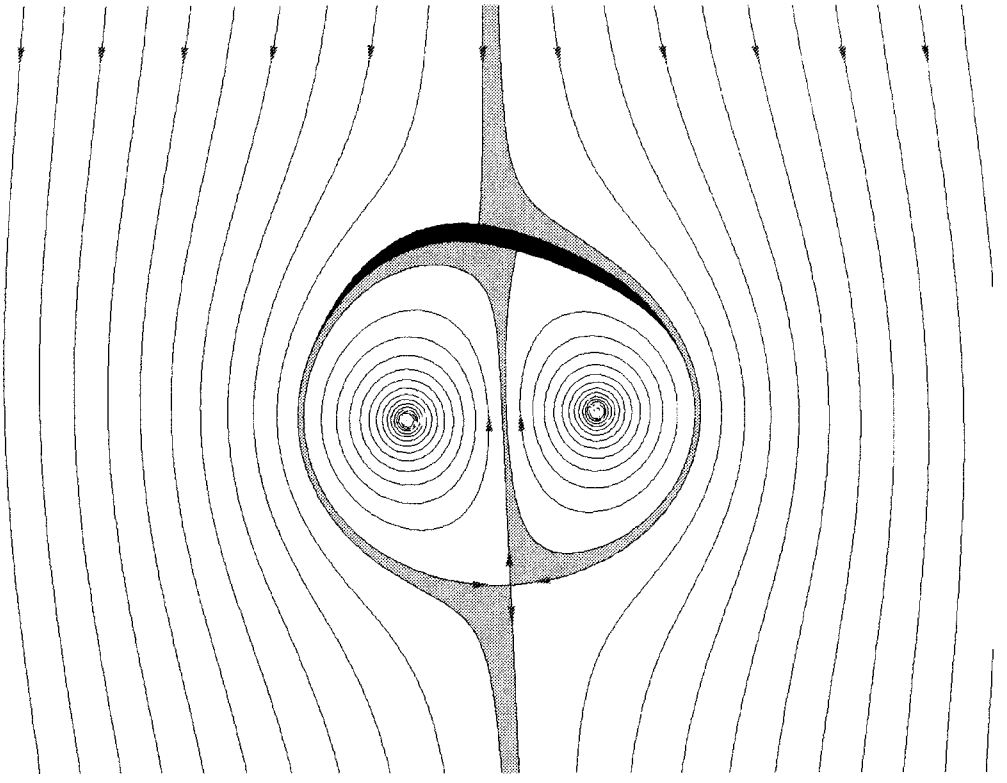

FIGURE 5. Profile and streamline pattern ($\epsilon = 0.5$, $\chi = 0.5$).

is cusped at the trailing edges z_{T_1}, z_{T_2}, as represented in figure 5 for $\epsilon = 0.5$, $\chi = 0.5$. These deformations can be replaced with any similar deformations. The lift obtained using this specific form of deformation is not large, but optimizing the deformation for achieving maximum lift is far beyond the scope of the present paper.

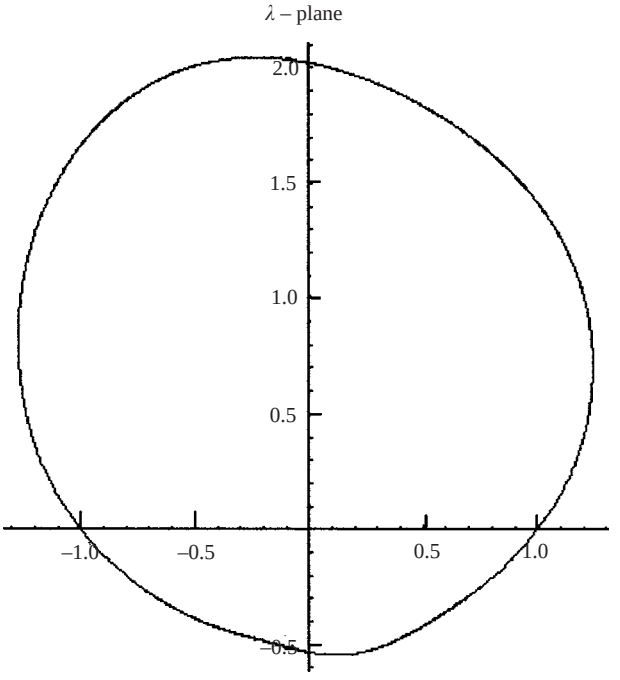

FIGURE 6. Quasi-circle in the λ-plane.

A mapping chain is used to map the z-plane profile onto the μ-plane unit circle. The transformation

$$z_1 = 4\frac{z - z_{T_2}}{z_{T_1} - z_{T_2}} - 2 \tag{4.4}$$

rescales the profiles bringing trailing edges into the real axes ($z_{T_1} \to 2$, $z_{T_2} \to -2$). The inverse Joukowski mapping

$$\lambda = \frac{z_1 + \sqrt{z^2 - 4}}{2} \tag{4.5}$$

transforms the profile into a quasi-circle in the λ-plane, as shown in figure 6.

The Theodorsen–Garrick transformation

$$\lambda = \mu \exp \sum_{j=0}^{\infty} (a_j + \mathrm{i}b_j)\mu^j \tag{4.6}$$

maps the domain external to the unit circle in the μ-plane into the domain external to the quasi-circle in the λ-plane.

The coefficients a_j, b_j in (4.6) are determined following the procedure described in detail by Ives (1976). Briefly, since the quasi-circle is a smooth line, the series can be truncated at a suitably large $j = N$ (in our computation we used $N = 400$), the a_j, b_j terms are then computed by a trial and error process. Let $\lambda = r\exp(\mathrm{i}\vartheta)$ and $\mu = \rho\exp(\mathrm{i}\varphi)$; the process is based on enforcing the correspondence between the λ-plane quasi-circle $r = r(\vartheta)$ and the μ-plane unit circle $\rho = 1$. A cubic spline is used to obtain a continuous representation of the quasi-circle, which is defined on a discrete set of points by the previous transformations. The unit circle of the λ-plane is divided into $2N$ intervals of $\Delta\varphi = 2\pi/(2N)$. The relationships between the $2N$ circle and quasi-circle points are then obtained by taking the real and imaginary part of

the logarithm of (4.6) for $\rho = 1$:

$$\log r(\vartheta_k) = \sum_{j=0}^{N} [a_j \cos(jk\Delta\varphi) + b_j \sin(jk\Delta\varphi)], \quad j = 0, \ldots, N;\ k = 0, \ldots 2N-1, \tag{4.7}$$

$$\vartheta_k = k\Delta\varphi + \sum_{j=0}^{N} [b_j \cos(jk\Delta\varphi) - a_j \sin(jk\Delta\varphi)], \quad j = 0, \ldots, N;\ k = 0, \ldots 2N-1. \tag{4.8}$$

The iterative process is started by assuming $\vartheta_k = \varphi_0 + k\,\Delta\varphi$, where φ_0 determines a rigid rotation of the μ-plane and can be chosen freely. Equation (4.7) then allows the computation of the $2N$ unknowns: a_j $(j = 0, \ldots N)$ and b_j $(j = 1, \ldots N-1)$. Coefficients b_0 and b_N are not among the unknowns of equation (4.7). In fact, b_0 is determined by (4.8) for $k = 0$: $b_0 = \varphi_0 - \sum_{j=1}^{N} b_j$, b_N is free and is set to zero to close the problem. Equation (4.8) can now yield a new set of ϑ_k values. The process is repeated until convergence is reached. The two steps of each cycle, i.e. a_j, b_j computation and ϑ_k evaluation, are efficiently accomplished by means of the FFT algorithm.

The mapping from the μ-plane to the z-plane, $z = z_f(\mu)$, is the chain formed by (4.6) and the inverse of functions (4.5) and (4.4), that is,

$$z = z_f(\mu) = z(z_1(\lambda(\mu))) \tag{4.9}$$

with

$$z_1(\lambda) = \lambda + \frac{1}{\lambda}, \quad z(z_1) = \frac{z_1 + 2(z_{T_1} + z_{T_2})}{4}.$$

4.3. *Complex potential*

The complex potential $w(\mu)$ is obtained on the μ-plane by superimposing a uniform flow, two free vortices external to the unit circle, their reflected images inside the circle, and a vortex located at the circle centre (see figure 7), that is,

$$w = Q_\infty \mu + \frac{Q_\infty^*}{\mu} + \frac{\kappa_1}{2\pi i} \log\left(\frac{\mu - \mu_1}{\mu - \bar{\mu}_1}\right) + \frac{\kappa_2}{2\pi i} \log\left(\frac{\mu - \mu_2}{\mu - \bar{\mu}_2}\right) + \frac{\gamma}{2\pi i} \log(\mu), \tag{4.10}$$

where an asterisk denotes the complex conjugate; $\bar{\mu}_{1,2} = 1/\mu_{1,2}^*$; κ_1, κ_2, μ_1, μ_2, are free vortex circulations and locations, respectively; γ is the circulation of the centre vortex, i.e. the total circulation; Q_∞ is the asymptotic complex velocity in the μ-plane:

$$Q_\infty = \mathrm{i}e^{-\mathrm{i}\alpha} \lim_{\mu \to \infty} \frac{\mathrm{d}z}{\mathrm{d}\mu}.$$

Since $\lim_{\mu\to\infty} z_f(\mu) = \infty$, the corresponding asymptotic velocity on the z-plane has a unit modulus and α is its incidence with respect to the negative imaginary direction.

Two Kutta–Joukowski conditions have to be satisfied at the circle points μ_{T_1}, μ_{T_2} which correspond to trailing edges z_{T_1}, z_{T_2}, that is,

$$\left(\frac{\mathrm{d}w}{\mathrm{d}\mu}\right)_{\mu_{T_1}} = 0, \quad \left(\frac{\mathrm{d}w}{\mathrm{d}\mu}\right)_{\mu_{T_2}} = 0. \tag{4.11}$$

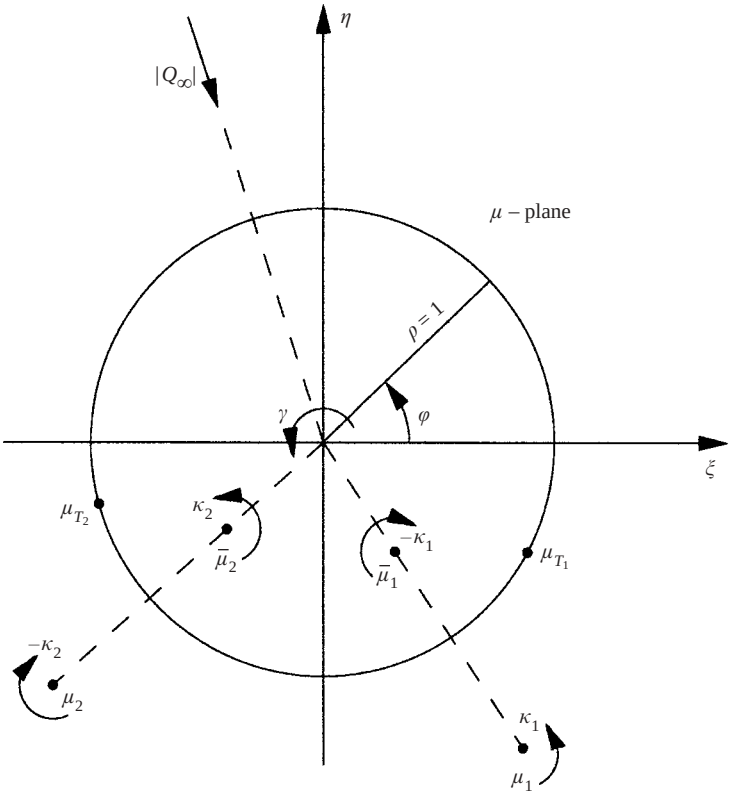

FIGURE 7. μ-plane.

Moreover, the free vortices located at $z_1 = z_f(\mu_1)$, $z_2 = z_f(\mu_2)$, have to be in equilibrium. According to the Routh rule (see Routh 1881; Clements 1973), the vortex velocity can be expressed as ($j = 1, 2$ here and below to the end of the subsection):

$$\dot{z}_j^* = \left\{ \left[\dot{\mu}_j^* - \frac{\kappa_j}{4\pi i} \frac{\mathrm{d}}{\mathrm{d}\mu} \left(\log \frac{\mathrm{d}z}{\mathrm{d}\mu} \right) \right] \frac{\mathrm{d}\mu}{\mathrm{d}z} \right\}_{\mu_j}, \tag{4.12}$$

where $\dot{\mu}_j^*$ is the velocity that is relevant to the free vortices on the μ-plane:

$$\dot{\mu}_j^* = Q_\infty - \frac{Q_\infty^*}{\mu_j^2} - \frac{\kappa_j}{2\pi i} \frac{1}{\mu_j - \bar{\mu}_j} + \frac{\kappa_l}{2\pi i} \left(\frac{1}{\mu_j - \mu_l} - \frac{1}{\mu_j - \bar{\mu}_l} \right) + \frac{\gamma}{2\pi i} \frac{1}{\mu_j} \quad (j = 1, 2;\ l \neq j).$$

The vortex equilibrium conditions are therefore

$$\dot{\mu}_j^* = \frac{\kappa_j}{4\pi i} \frac{\mathrm{d}}{\mathrm{d}\mu} \left(\log \frac{\mathrm{d}z}{\mathrm{d}\mu} \right)_{\mu_j}. \tag{4.13}$$

The flow velocity at the trailing edges $V_p(\mu_{T_j})$ is

$$V_p(\mu_{T_j}) = \lim_{\mu \to \mu_{T_j}} \frac{\mathrm{d}w/\mathrm{d}\mu}{\mathrm{d}z/\mathrm{d}\mu} = \left(\frac{\mathrm{d}^2 w/\mathrm{d}\mu^2}{\mathrm{d}^2 z/\mathrm{d}\mu^2} \right)_{\mu_{T_j}}$$

and the derivative of the flow velocity $\partial|V_p|/\partial\varphi$ can be deduced from the Cauchy–Riemann conditions:

$$\left(\frac{\partial \log|V_p|}{\partial\varphi}\right)_{\mu_{T_j}} = -\lim_{\mu\to\mu_{T_j}} \mathrm{Im}\left[\mu\frac{\mathrm{d}}{\mathrm{d}\mu}\left(\log\frac{\mathrm{d}w/\mathrm{d}\mu}{\mathrm{d}z/\mathrm{d}\mu}\right)\right]$$
$$= -\mathrm{Im}\left(\mu\frac{\mathrm{d}^3w/\mathrm{d}\mu^3 - V_p\mathrm{d}^3z/\mathrm{d}\mu^3}{2\,\mathrm{d}^2w/\mathrm{d}\mu^2}\right)_{\mu_{T_j}}. \tag{4.14}$$

4.4. *Flow configuration with a favourable pressure gradient throughout*

The flow depends on $\alpha,\ \gamma,\ \kappa_1,\ \kappa_2,\ \mu_1 = \xi_1 + \mathrm{i}\,\eta_1,\ \mu_2 = \xi_2 + \mathrm{i}\,\eta_2$, that is, on eight real parameters, and has to satisfy equations (4.11) and (4.13), which are equivalent to six real equations; as a consequence the flow has two degrees of freedom.

We chose (α, γ) as the parameters that define the flow configuration space. Free vortex circulations κ_1, κ_2 can be expressed in closed form as explicit functions of the other parameters by using the Kutta–Joukowski conditions (4.11) and thus be eliminated from (4.13) which, given (α, γ) values, are solved numerically providing free vortex equilibrium locations $\mu_1 = \xi_1 + \mathrm{i}\,\eta_1,\ \mu_2 = \xi_2 + \mathrm{i}\,\eta_2$. A conjugate gradient method (Polak 1971) has been adopted to obtain favourable-pressure-gradient flow configurations (α, γ) that fulfil the two necessary conditions (2.5). The fact that the pressure gradient is favourable everywhere on the body surface has been verified *a posteriori*. We considered the function

$$\mathscr{F} = \tfrac{1}{2}\left(L_1^2 + L_2^2\right) \tag{4.15}$$

with

$$L_j = \left(\frac{1}{|V_p|}\frac{\partial|V_p|}{\partial\varphi}\right)_{\mu_{T_j}} \qquad (j = 1, 2) \tag{4.16}$$

given by (4.14). The analytically computed gradient $(\partial\mathscr{F}/\partial\alpha, \partial\mathscr{F}/\partial\gamma)$ provides the path to be followed in the (α, γ) space to find minimum $\mathscr{F}$. We expect $\mathscr{F} = 0$ at the minimum.

4.4.1. *Gradient evaluation*

According to (4.10), (4.14), (4.15), and (4.16), once κ_1, κ_1 are eliminated as mentioned, the functional $\mathscr{F}$ depends on (α, γ) directly and, through vortex equilibrium locations $\xi_j(\alpha, \gamma)$, $\eta_j(\alpha, \gamma)$, indirectly. The functional gradient is therefore

$$\frac{\partial\mathscr{F}}{\partial\alpha} = \mathscr{F}_{\partial\alpha} + \sum_{l=1}^{2}\left(\mathscr{F}_{\partial\xi_l}\frac{\partial\xi_l}{\partial\alpha} + \mathscr{F}_{\partial\eta_l}\frac{\partial\eta_l}{\partial\alpha}\right), \quad \frac{\partial\mathscr{F}}{\partial\gamma} = \mathscr{F}_{\partial\gamma} + \sum_{l=1}^{2}\left(\mathscr{F}_{\partial\xi_l}\frac{\partial\xi_l}{\partial\gamma} + \mathscr{F}_{\partial\eta_l}\frac{\partial\eta_l}{\partial\gamma}\right).$$

Differentiation of the vortex equilibrium conditions $\dot{x}_j - i\,\dot{y}_j = \dot{z}_j^* = 0$, with $\dot{z}_j^*$ expressed using (4.12), yields the linear systems

$$\sum_{l=1}^{2}\left(\frac{\partial\dot{x}_j}{\partial\xi_l}\frac{\partial\xi_l}{\partial\alpha} + \frac{\partial\dot{x}_j}{\partial\eta_l}\frac{\partial\eta_l}{\partial\alpha}\right) = -\dot{x}_{j_{\partial\alpha}}, \qquad \sum_{l=1}^{2}\left(\frac{\partial\dot{y}_j}{\partial\xi_l}\frac{\partial\xi_l}{\partial\alpha} + \frac{\partial\dot{y}_j}{\partial\eta_l}\frac{\partial\eta_l}{\partial\alpha}\right) = -\dot{y}_{j_{\partial\alpha}} \quad (j = 1, 2)$$

$$\sum_{l=1}^{2}\left(\frac{\partial\dot{x}_j}{\partial\xi_l}\frac{\partial\xi_l}{\partial\gamma} + \frac{\partial\dot{x}_j}{\partial\eta_l}\frac{\partial\eta_l}{\partial\gamma}\right) = -\dot{x}_{j_{\partial\gamma}}, \qquad \sum_{l=1}^{2}\left(\frac{\partial\dot{y}_j}{\partial\xi_l}\frac{\partial\xi_l}{\partial\gamma} + \frac{\partial\dot{y}_j}{\partial\eta_l}\frac{\partial\eta_l}{\partial\gamma}\right) = -\dot{y}_{j_{\partial\gamma}} \quad (j = 1, 2)$$

solution of which provides the derivatives $\partial\xi_j/\partial\alpha$, $\partial\eta_j/\partial\alpha$, $\partial\xi_j/\partial\gamma$, $\partial\eta_j/\partial\gamma$.

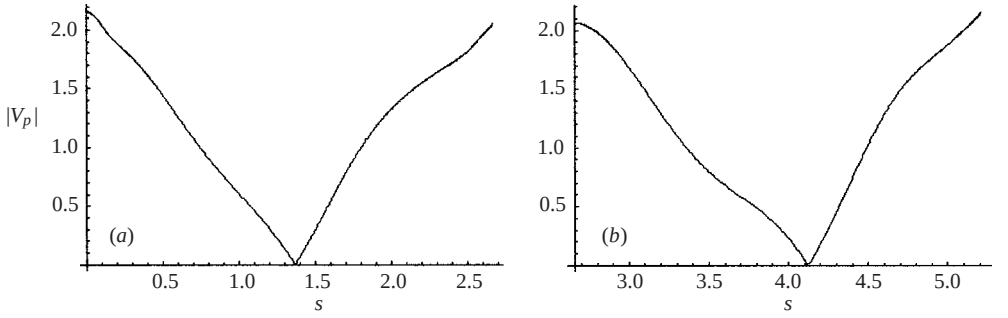

FIGURE 8. $|V_p|$ versus s for $\gamma = 0$, $\alpha = 0$. (a) Profile upper side, (b) lower side.

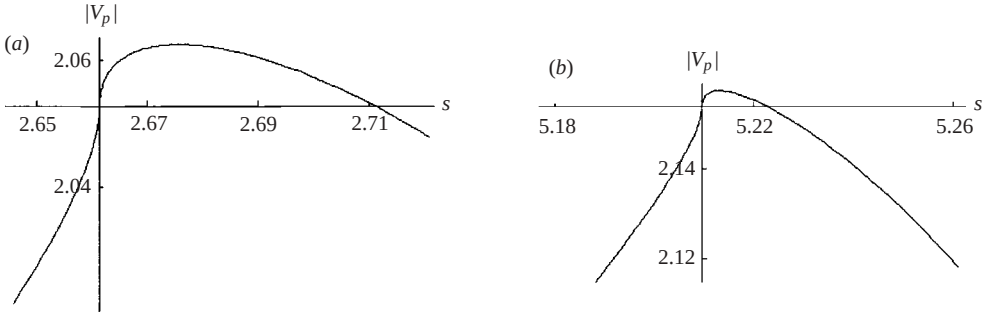

FIGURE 9. Close-up of $|V_p|$ versus s for $\gamma = 0$, $\alpha = 0$ at $z = z_{T_2}$ (a) and $z = z_{T_1}$ (b).

4.5. *Numerical examples*

The computations presented hereafter, including symbolic manipulations and differentiations, have been carried out automatically using the *Mathematica* package.

First, the general flow past the body described in § 4.2 (see figure 5) is presented, without the requirement that the pressure gradient be everywhere favourable. Then, for the same body, a flow configuration with everywhere-favourable pressure gradient is sought and the outcome is presented. In § 4.6 an assessment of the overall computational accuracy is presented.

We first consider the flow configuration that corresponds to zero circulation and zero incidence, $\gamma = 0$, $\alpha = 0$. The value of functional (4.15) is $\mathscr{F} = 0.00356193$ with $L_1 = 0.0494094$ and $L_2 = 0.0684292$. The necessary condition (2.5) for a favourable pressure gradient on the profile contour is violated at both trailing edges and, according to (2.6), the flow velocity $|V_p|$ has an infinite gradient which implies acceleration on one side and deceleration on the other side of each trailing edge, as discussed in § 2.2.

The velocity distribution on the profile sides is plotted in figure 8 versus the arclength

$$s = \int_{\varphi_{\mu_{T_1}}}^{\varphi} |\mathrm{d}z/\mathrm{d}\mu| d\varphi'.$$

At a first glance it seems favourable everywhere, but on looking closer it can be seen that due to infinite gradients the maximum values are not attained at the trailing edges. A closer look at the velocity distribution on the lower and upper sides of the trailing edges plotted in figure 9 shows that the local velocity maxima are not attained

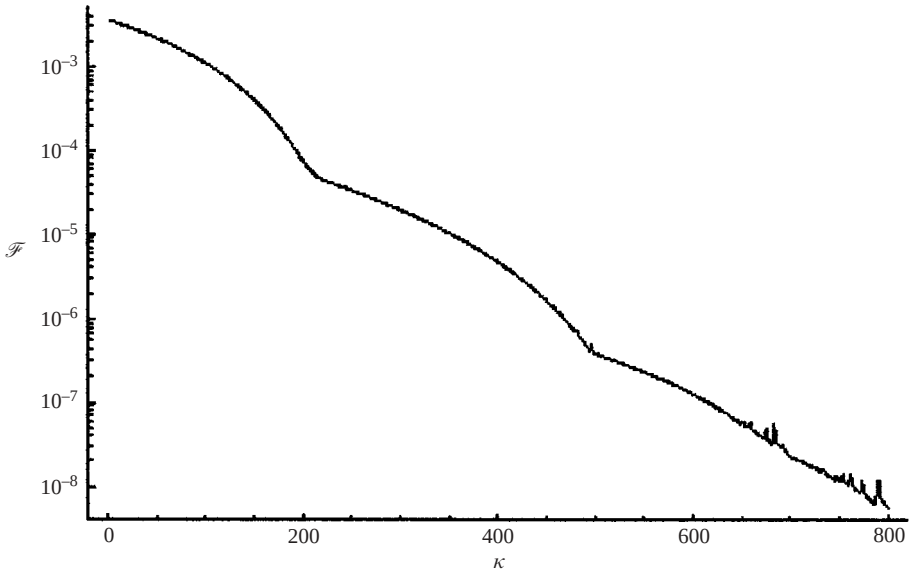

FIGURE 10. Functional $\mathscr{F}$ history.

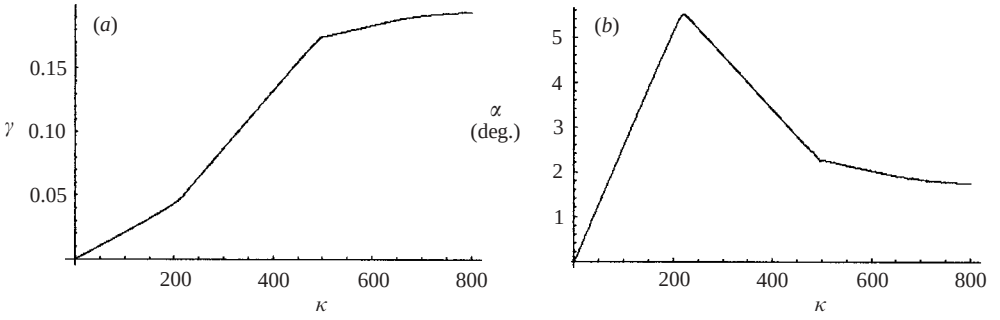

FIGURE 11. (*a*) γ, (*b*) α history.

at the edges. If the viscosity were taken into account, boundary layer separation would be inevitable due to infinite pressure gradient. Once triggered, separation can then spread over a large part of the airfoil.

The descent method described in § 4.4 was used to determine the flow configuration (γ, α) that minimizes the functional $\mathscr{F}$. The $\mathscr{F}$ descent history is plotted versus iteration steps in figure 10. A fixed descent step is performed, i.e. no line search is performed in the descent direction. The descent step is adapted by decreasing its value according to the reduction in $\mathscr{F}$. The slope change in the history is due to the change in the descent step. As shown in figure 10, the computation was terminated when the functional $\mathscr{F}$ decreased from $O(10^{-3})$ to $O(10^{-9})$ with trailing-edge derivatives $\partial|V_p|/\partial\varphi$ decreasing from $O(10^{-2})$ to $O(10^{-6})$. The functional gradient is $O(10^{-5})$. The circulation γ and incidence α histories are drawn in figure 11; they reach the values $\gamma = 0.19446$, $\alpha = 1.7383°$, to which $\mu_1 = 1.49125\exp(\mathrm{i}\,5.03613)$, $\mu_2 = 1.54888\exp(-\mathrm{i}\,1.87583)$, $\kappa_1 = -5.92435$, $\kappa_2 = 6.02955$ correspond. By virtue of the Joukowski theorem the circulation γ also gives the lift.

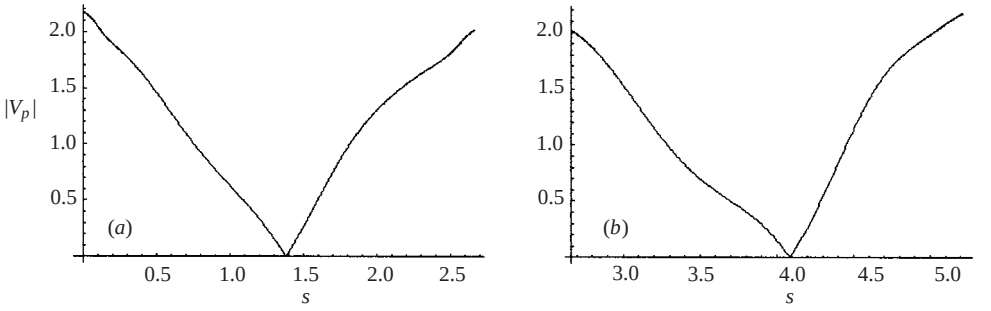

FIGURE 12. $|V_p|$ versus s for $\gamma = 0.19446$, $\alpha = 1.7383°$. (a) Profile upper side, (b) lower side.

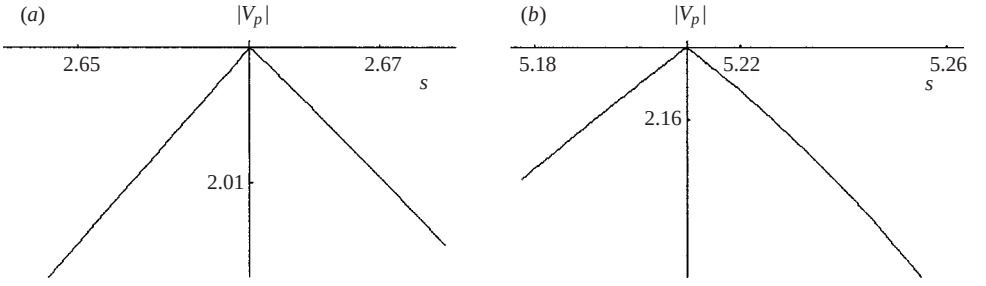

FIGURE 13. Close-up of $|V_p|$ versus s for $\gamma = 0.19446$, $\alpha = 1.7383°$ at (a) $z = z_{T_2}$ and (b) $z = z_{T_1}$.

As can be seen in figure 10, functional $\mathscr{F}$ could be driven to further smaller values, but the goal of everywhere accelerating flow has already been numerically achieved. The velocity distribution on the profile's upper and lower sides is plotted in figure 12. It is quite similar to that of figure 8, but a comparison of the trailing-edge close-ups, shown in figure 13, with those of figure 9, confirm the substantial achievement of the goal. The analysis of a potential flow past a cusp presented in § 2.2 is confirmed, since the velocity distribution has infinite gradients when condition (2.5) is not satisfied, while it tends to have finite discontinuous gradients, with opposite values, when the trailing-edge maximum velocity is approached.

4.6. *Validation and accuracy*

The main result of the present paper is of a qualitative nature: it can be asserted that a lifting body of non-zero volume exists with a favourable pressure gradient over its entire surface if two trapped point vortices are present in the flow. This qualitative conclusion is however based on a numerical result. Hence, two questions should be addressed, namely the validity of our code and the accuracy of the result.

The code was validated by calculating the same flow using a quite different method: the vortex-panel code used in Bunyakin *et al.* (1998) was modified to incorporate two point vortices with known positions. The vortex positions were then taken from the present calculations, and the velocity distribution on the body surface obtained with the modified code was compared with results obtained using the approach described here. The velocity at the vortex positions (which should be zero) was also calculated. The agreement was quite satisfactory.

Regarding the accuracy of the specific results presented here, we can say that the described flow computations are almost fully analytical, with the exceptions of the

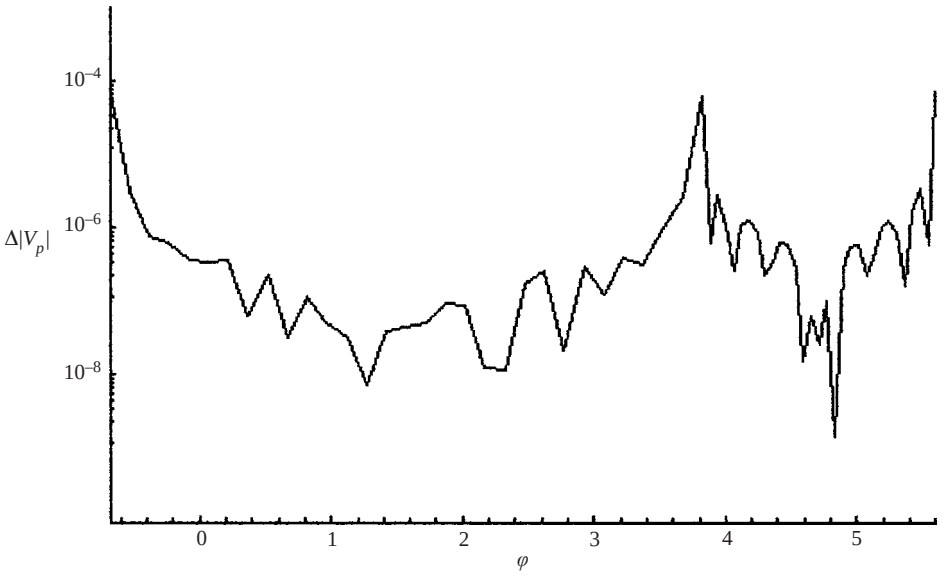

FIGURE 14. $\|V_p| - |V_{th}\|$ versus φ.

Theodorsen–Garrick mapping which involves the use of a cubic spline, as described in § 4.2. Nevertheless, a test has been performed to check the accuracy. The flow past an undeformed separatrix arc of a vortex pair flow can be assumed as a benchmark of the process based on conformal mapping, since the configuration corresponding to $\gamma = 0$, $\alpha = 0$ can also be computed directly from (4.1).

The undeformed separatrix arc at the basis of the above examples, shown in figure 4, has been selected for this test. The discrete representation of the arc, as required by the conformal mapping process, was based on 800 points, as in the above examples. The difference $\|V_p|(\varphi) - |V_{th}|(\varphi)|$ is plotted in figure 14. According to (4.1) and (4.9), $|V_{th}|(\varphi)$ is given by

$$|V_{th}|(\varphi) = \left| \mathrm{i} + \frac{\kappa}{2\pi \mathrm{i}} \left(\frac{1}{z - x_0} - \frac{1}{z + x_0} \right) \right|_{z = z_f[\exp(\mathrm{i}\varphi)]}$$

The errors of the free vortex intensities are $O(10^{-7})$ and the errors of equilibrium locations are $O(10^{-8})$. For $\gamma = 0$, $\alpha = 0$ the flow configuration is always of a favourable pressure type, functional $\mathscr{F}$ in (4.15) should be zero, and the computed value is $O(10^{-8})$.

These checks show that the obtained result is sufficiently reliable.

5. Discussion

It can seem that the problem of flows with trapped vortices is not realistic. Trapped vortices have however already been successfully used to prevent separation from the surface for an experimental aircraft EKIP, see further references in Bunyakin *et al.* (1998). It is therefore important to discuss the relationship between the simplified model of the present paper and realistic flows of the same type.

First, there are no point vortices in a real flow. Instead, the vorticity is distributed over the eddy. Point vortices, however, can be considered as an approximation for small regions of distributed vorticity. Hence, in view of the result of the present paper,

it is natural to expect that there are bodies with a favourable pressure gradient in the case of two distributed trapped vortices.

Second, a real flow at a high Reynolds number is turbulent. As was pointed out by Wu & Wu (1992), turbulence itself does not interfere with the idea of a trapped vortex. Boundary layers and mixing layers at the eddy boundary can be turbulent without a large increase in drag and decrease in lift, provided that the large-scale eddies remain attached to the body. Turbulence will nonetheless affect the characteristics of such eddies. However, theoretical analysis of turbulent flows with trapped vortices should be preceded by experiments and numerical calculations aimed at finding the appropriate turbulence model.

Third, such flows, even if modelled with point vortices, are generally not stable with respect to large-scale vortex shedding. If the point vortices calculated in the present paper were displaced even slightly, they would move and, quite likely, would eventually leave the vicinity of the body, and the flow in the vicinity of the body would become purely potential, with infinite velocities at the sharp edges. In a more realistic model and in reality the new vorticity would then be shed from the body, and the entire process would repeat itself.

Fourth, in the present paper the vortex circulations and the total circulation were adjusted so as to satisfy the Kutta–Joukowski conditions at the sharp edges and the necessary condition for a favourable pressure gradient. In reality, the amount of vorticity in the eddy and the total circulation are determined by viscous effects. As is known, these effects do in fact lead to the Kutta–Joukowski conditions being satisfied. However, the necessary condition for a favourable pressure gradient, that is (2.5), cannot be expected to be satisfied automatically due to the action of viscosity. With viscosity taken into account one would have to add an additional parameter for the body shape and adjust this parameter to satisfy the necessary condition for a favourable pressure gradient.

Hence, as the possibility of designing a body with a favourable pressure gradient has been demonstrated in principle, further theoretical studies may involve solving the following two problems.

First, the major question concerns the control of the large-scale instability. Recent successes in active flow control would seem to offer some hope in this respect (see, for example, Min & Choi 1999).

Second, let us now assume that such active control is implemented and, for simplicity, that the flow is laminar and steady. Then a more realistic model of the flow should take viscosity into account. The appropriate tool for this is the high-Reynolds-number-asymptotic method. Asymptotic solutions have so far been obtained for flows with a single trapped vortex (Bunyakin *et al.* 1998) and for a symmetric flow past a bluff body (see Chernyshenko 1998). However, the flow with two vortices poses, somewhat unexpectedly, a new and challenging problem. In the high-Reynolds-number limit, the flow with two trapped vortices should normally correspond to the Batchelor model. This means that the vorticity should be constant (but perhaps different) inside each eddy, and that the tangential velocity may be discontinuous across the eddy boundaries. For a given body shape and in a non-symmetrical case, as is necessary for a lifting body, such an inviscid flow could be expected to be uniquely determined by five parameters, once the incidence is fixed, for example by two eddy vorticities, two positions of separation points on the body surface, and the total circulation. Existing theories provide certain viscous mechanisms for eliminating the non-uniqueness of the inviscid flow, that is, a certain condition has to be satisfied for the solution in the cyclic boundary layer surrounding the eddy to exist, and

another condition is provided by the local analysis of the flow in the vicinity of the separation point. For the case when there is a sharp corner on the body, this local condition is equivalent to the Kutta–Joukowski condition. Further details can be found in the previously mentioned papers, and we also note that here we have ignored the (very difficult) problem of secondary separation, that is the separation from inside the cavity, addressed in Bunyakin *et al.* (1998). These mechanisms are sufficient to determine the unique solution in the case of a symmetrical flow past a bluff body or a flow with a single trapped vortex. In the configuration in question, they are not sufficient. Here there are two cyclic layers and two separation points which allow one to determine four parameters, but the inviscid flow depends on five parameters, and a one-parameter set of solutions exists as in § 4.4.

We are therefore faced with an interesting problem which has not attracted much attention so far. It would be highly desirable to understand at least the physical mechanism that determines the fifth parameter, and the laminar steady high-Reynolds-number asymptotic approach seems to be the best tool for revealing this mechanism. One feature of the streamline pattern in figure 5 may suggest a possible mechanism. Figure 5 shows that one of the closed streamline regions (left) is not in contact with the wall. It is separated from the wall by a narrow strip (coloured grey in the figure) of fluid between two streamlines coming from and going to infinity. Such a configuration presumably cannot be a limit of a viscous flow. Indeed, since all the streamlines within that strip come from infinity, in the limiting flow vorticity is zero inside this region. However, due to viscous diffusion, the vorticity from the closed streamline region will slowly diffuse outside. Another way to see it is to apply the maximum principle to the viscous vorticity equation and then take a limit of zero viscosity. By the maximum principle vorticity inside a closed contour is always between its maximum and minimum on the contour, and so it will be in the limit, too. Taking this contour to be entirely inside the grey area in figure 5 proves that the vorticity inside the closed streamline region surrounded by purely potential flow should be zero. Therefore, viscous flow analysis can give an additional requirement on the topology of the flow and this can provide the fifth necessary condition. However, any final conclusions on such a difficult matter should be made only after much more careful and extensive study.

The main result of the present paper is that in principle flows past lifting bodies with a favourable pressure gradient on the entire body surface are possible, if two trapped vortices are present. This result gives rise to new problems, in particular active control of the flows with trapped vortices and a high-Reynolds number asymptotic theory of separated flows past non-symmetric bodies.

The research collaboration that resulted in the present paper was in part supported by the Royal Society grant under the European Science Exchange Programme.

REFERENCES

Avhadief, F. G. & Maklakov, D. V. 1995 A theory of pressure envelopes for hydrofoils. *Ship Technol. Res.* **42**, 81–102.

Baranov, P. A., Guvernyuk, S. V., Zubin, M. A. & Isaev, S. A. 2000 Numerical and physical modeling of the circulation flow in a vortex cell in the wall of a rectilinear channel. *Izv. RAN, Mekh. Zhid. i Gaza*, No. 5, 44–55 (in Russian, English transl. *Fluid Dyn.* 2000 **35**(5), 663–673).

Batchelor, G. K. 1956 A proposal concerning laminar wakes behind bluff bodies at large Reynolds number. *J. Fluid Mech.* **1**, 388–398.

Bunyakin, A. V., Chernyshenko, S. I. & Stepanov, G. Yu. 1998 High-Reynolds-number Batchelor-model asymptotics of a flow past an airfoil with a vortex trapped in a cavity. *J. Fluid Mech.* **358**, 283–297.

Chernyshenko, S. I. 1995 Stabilization of trapped vortices by alternating blowing-suction. *Phys. Fluids* **7**, 802–807.

Chernyshenko, S. I. 1998 Asymptotic theory of global separation. *Appl. Mech. Rev.* **9**, 523–536.

Clements, R. R. 1973 An inviscid model of two-dimensional vortex shedding. *J. Fluid Mech.* **57**, 321–336.

Courant, R. 1962 *Partial Differential Equations*. Interscience.

Elizarov, A. M., Il'inskiy, N. B. & Potashev, A. V. 1997 *Mathematical Methods of Airfoil Design*. Akademie Verlag, Berlin.

Huang, M. K. & Chow, C. Y. 1982 Trapping of a free vortex by Joukowski airfoils. *AIAA J.* **20**, 292–298.

Galletti, B., Iollo, A. & Zannetti, L. 2002 Aerodynamic constraints for vortex trapping airfoils. *Accademia delle Scienze di Torino – Atti Scienze Fisiche* **136**, 21–30.

Iollo, A. & Zannetti, L. 2000 Optimal control of a vortex trapped by an airfoil with a cavity. *Flow, Turbulence Combust.* **65**, 417–430.

Ives, D. C. 1976 A modern look at conformal mapping, including multiply connected regions. *AIAA J.* **14**, 1006–1011.

Lighthill, M. J. 1945 A new method of two-dimensional aerodynamic design. *Aero. Res. Counc. R&M* 2104.

Min, C. & Choi, H. 1999 Suboptimal feedback control of vortex shedding at low Reynolds numbers. *J. Fluid Mech.* **401**, 123–156.

Polak, E. 1971 *Computational Methods in Optimization: A Unified Approach*. Academic.

Rossow, V. J. 1978 Lift enhancement by an externally trapped vortex. *J. Aircraft* **15**, 618–625.

Routh, E. J. 1881 Some applications of conjugate functions. *Proc. Lond. Math. Soc.* **12**.

Saffman, P. G. & Sheffield, J. S. 1977 Flow over a wing with an attached free vortex. *Stud. Appl. Maths* **57**, 107–117.

Wu, J. M. & Wu, J. Z. 1992 Vortex lift at a very high angle of attack with massively separated unsteady flow. In *Fluid Dynamic of High Angle of Attack. IUTAM Symp. Tokyo, Japan, September 13–17, 1992* (ed. R. Kawamura & Y. Aihara), p. 34. Springer.

Wu, J. Z., Lu, X. Y., Denny, A. G., Fan, M. & Wu, J. M. 1998 Post-stall flow control on an airfoil by local unsteady forcing. *J. Fluid Mech.* **371**, 21–58.